slightly lengthened, with a concomitant shortening of B–B bonds and a consequential reduction of the CCB angles in the ring plane.

The trimethylsilyl group has C(cage)SiC(Me) angles much greater than C(Me)SiC(Me) (114 and 105°, respectively), but otherwise there is no sign of steric strain in the molecule. The two types of Si–C bond have essentially the same length. The preferred conformation has one Si–C(Me) bond eclipsing the ring C–C bond. A conformation in which an Si–C(Me) bond eclipsed a ring C–B bond also gave an R factor minimum, but it was significantly worse than the favored conformation. In this form the BCCSi dihedral angle went down to 164°, so that the trimethylsilyl group lay well below the plane of the ring atoms. Of course, it may be that there is fairly free rotation about the Si–C bond, but we have not considered models in which more than one conformer is present at one time.

Acknowledgment. This work was supported by the National Science Foundation under Grant No. CHE-84-18874, the donors of the Petroleum Research Fund, administered by the American Chemical Society, and the Robert A. Welch Foundation under Grant No. N-1016. We thank Professor John A. Maguire for helpful suggestions concerning this work. D.W.H.R. thanks the Science and Engineering Research Council for financial support.

Registry No. I, 91686-41-8; II, 31259-72-0.

Contribution from the Fachbereich Chemie, Johannes-Gutenberg-Universität, D-6500 Mainz, FRG

Structure Determination and Investigation of the High-Spin ↔ Low-Spin Transition of $[Fe(2\text{-pic})_3]Br_2 \cdot EtOH$†

L. Wiehl, G. Kiel, C. P. Köhler,‡ H. Spiering, and P. Gütlich*

Received July 30, 1985

A single-crystal X-ray diffraction analysis was carried out on the spin-crossover compound $[Fe(2\text{-pic})_3]Br_2 \cdot EtOH$ (2-pic = 2-(aminomethyl)pyridine) in the temperature region between room temperature and 110 K. $[Fe(2\text{-pic})_3]Br_2 \cdot EtOH$ crystallizes monoclinically ($Z = 4$) in the space group $P2_1/n$ (No. 14) with lattice constants $a = 11.164$ (12) Å, $b = 22.281$ (16) Å, $c = 11.713$ (12) Å, $\beta = 118.02$ (5)°, and $V = 2572$ (5) Å^3 at 215 K. The structure in the high-spin state at 215 K was refined to a reliability index of $R = 0.050$ ($R_w = 0.076$). The dependence of the lattice dimensions on temperature is expressed in terms of the tensor of thermal expansion α and a deformation tensor ϵ due to the high-spin ↔ low-spin transition. The high-spin fraction $\gamma(T)$ was determined by susceptibility and Mössbauer measurements. $\gamma(T)$ shows a hysteresis of 2 K width. The X-ray structure was also investigated at 124 K, below the hysteresis region, and is isomorphous to the high-spin structure at 215 K. This compound is the first example that shows hysteresis in $\gamma(T)$ without a structural phase transition.

Introduction

The temperature-dependent low-spin (LS) ↔ high-spin (HS) transition has been the subject of increasing interest in recent years. The number of systems exhibiting this phenomenon is continuously growing, and several theoretical models have been published.[1-3] The models have in common that the interaction between the LS and HS complexes, which is cooperative in nature, is considered as an elastic interaction as a result of the change of the size of the complexes on going from LS to HS and of the shape of the complexes. Qualitatively, all types of observed transition curves can be reproduced theoretically, ranging from very gradual transition curves to those exhibiting hysteresis typical for first-order thermodynamic transitions. On the grounds of these theoretical models, changes of the crystal structure are driven by the spin change of the complex molecules, whereas earlier papers argued in the opposite direction; for example, order–disorder phenomena[4] or, especially, the structural changes accompanying transitions with hysteresis were considered as the primary phenomenon. This view seemed to be supported by the entropy changes involved. The spin change from $S = 0$ to $S = 2$ in the case of an octahedrally coordinated Fe^{2+} ion results in an entropy change of $\Delta S = -Nk_B \ln 5 = 14$ J mol^{-1}, which is to be compared with values of about 50 J mol^{-1} K^{-1} obtained[5] from calorimetric measurements in $[Fe(phen)_2(NCS)_2]$. The main part of ΔS obviously stems from changes of vibrational frequencies and not from the spin change.

In the theoretical model,[3] which has been successfully applied to the gradual spin transition in the mixed-crystal system $[Fe_xM_{1-x}(2\text{-pic})_3]Cl_2 \cdot EtOH$ (2-pic = 2-picolylamine = 2-(aminomethyl)pyridine; M = Zn,[3] M = Co[6]), the whole cationic complex molecule is considered rather than the isolated central metal ion. In that case, the change of the intramolecular vibrational frequencies, which has been observed by far-IR spectroscopy[7,8] for such systems, turns out to be the main contribution to the total entropy change. In view of this model it is justified to consider the change of the spin state and along with it the changes in size and shape of the cationic complex to be the driving force of the cooperative spin transition.

In order to support this conception experimentally, we looked for a HS/LS system that undergoes a first-order phase transition with a hysteresis but that is not accompanied by a structural phase transition of the lattice. In the course of our systematic investigation of the system $[Fe_xM_{1-x}(2\text{-pic})_3]Cl_2 \cdot EtOH$, we found that the interaction constant $\Gamma(x = 1)$ in the equation of the free energy f per isolated complex molecule[3]

$$f = f_0(\gamma) + \Delta(x)\,\gamma - \Gamma(x)\,\gamma^2 \qquad (1)$$

(f_0 is the free energy of isolated complexes, $\Delta(x)$ is an energy shift proportional to the concentration x, γ is the HS fraction) is just below the value that gives rise to a hysteresis in the curve of the HS fraction $\gamma(T)$. Γ is interpreted in the frame of elasticity theory. It depends on the volume V_c and the volume change ΔV_{HL} of the crystal per formula on going from the LS to the HS state, the bulk modulus K, and the Eshelby constant γ_0:[3]

$$\Gamma(x) = \frac{1}{2}xK\frac{\Gamma_0 - 1}{\Gamma_0}\frac{(\Delta V_{HL})^2}{V_c} \qquad (2)$$

† Dedicated to Professor Gerhard Gattow on the occasion of his 60th birthday.

‡ In partial fulfillment of the Ph.D. Thesis.

(1) Kambara, T. *J. Phys. Soc. Jpn.* **1980**, *49*, 1806.
(2) Ohnishi, S.; Sugano, S. *J. Phys. C* **1981**, *14*, 39.
(3) Spiering, H.; Meissner, E.; Köppen, H.; Müller, E. W.; Gütlich, P. *Chem. Phys.* **1982**, *68*, 65.
(4) Mikami-Kido, M.; Saito, Y. *Acta Crystallogr., Sect. B: Struct. Crystallogr. Cryst. Chem.* **1982**, *B38*, 452.
(5) Sorai, M.; Seki, S. *J. Phys. Chem. Solids* **1974**, *35*, 555.
(6) Sanner, I.; Meissner, E.; Köppen, H.; Spiering, H.; Gütlich, P. *Chem. Phys.* **1984**, *86*, 227.
(7) Müller, E. W.; Ensling, J.; Spiering, H.; Gütlich, P. *Inorg. Chem.* **1983**, *22*, 2074.
(8) Takemoto, J. H.; Hutchinson, B. *Inorg. Chem.* **1973**, *12*, 705.

0020-1669/86/1325-1565$01.50/0 © 1986 American Chemical Society

Table I. Crystal Data of $[Fe(2\text{-pic})_3]Br_2 \cdot EtOH$ at 215 K

cryst shape	short columns parallel to $\vec{a}$ faces {021}, {$\bar{1}$01}
cryst size	0.2 × 0.2 × 0.2 mm³
cryst syst	monoclinic
space group	$P2_1/n$ ($Z = 4$)
unit cell dimens (at 215 K)	a = 11.164 (12) Å b = 22.281 (16) Å c = 11.713 (12) Å β = 118.02 (5)°
volume of unit cell	V = 2572 (5) Å³
fw	586.14 ($FeN_6C_{20}OH_{30}Br_2$)
density (215 K)	$d_{X\text{-ray}}$ = 1.514 g/cm³
density (293 K)	$d_{X\text{-ray}}$ = 1.491 g/cm³, d_{exptl} = 1.490 g/cm³
symmetry positions	1: x, y, z 2: $0.5 + x, 0.5 - y, 0.5 + z$ 3: $-x, -y, -z$ 4: $0.5 - x, 0.5 + y, 0.5 - z$
no. of measd reflcns	8024
no. of unique reflcns ($I > 2\sigma(I)$)	4242 (12 observables/parameter)
reliability index	R = 0.050 R_w = 0.076

Small changes in K, γ_0, or V_c in suitable directions may therefore change $\Gamma(x = 1)$ to a slightly larger value and produce a hysteresis in $\gamma(T)$. We replaced the Cl^- ion by the larger Br^- in this compound and found indeed a small hysteresis of only 2 K width. This hysteresis has not been found in an earlier susceptibility study by Greenaway et al.[9] Therefore, we have performed a detailed X-ray study on this compound. The results will be compared with those of the chloride compound, which were first published by Greenaway et al.[9] and Mikami et al.[10] and later completed in our laboratory.[11]

Experimental Section

1. Chemical Preparations. The title compound was precipitated by reaction of excess picolylamine ($C_6N_2H_8$) with $FeBr_2 \cdot 4H_2O$ in ethanol under argon atmosphere, dried, and recrystallized from absolute ethanol (free from O_2 and H_2O). Anal. Calcd: C, 40.96; N, 14.33; H, 5.12. Found: C, 40.53; N, 14.38; H, 5.07. The yellow-brown crystals had the shape of short columns parallel to the $\vec{a}$ axis with main faces {021} and {$\bar{1}$01} and good cleavage along ($\bar{1}$01). The crystals for the X-ray measurements were mounted on glass fibers and sealed in glass capillaries.

2. X-ray Measurements. The monoclinic symmetry and the size of the unit cell were obtained from rotation and Weissenberg photographs at room temperature. The systematic absences ($(0k0)$ with $k = 2n$ and $(h0l)$ with $h + l = 2n$ present) lead to the space group $P2_1/n$ (standard setting is $P2_1/c$, No. 14). Weissenberg photographs at about 110 K verify that these absences occur also in the low-spin state.

Intensity data were collected by employing a four-circle diffractometer (CAD4/Enraf-Nonius) at two temperatures, the first set (8024 reflections) at 215 K and the second set (3928 reflections) at 124 K, just below the hysteresis but in the spin-transition region at a HS fraction of $\gamma = 0.5$ (cf. Figure 6). Measurements were performed with Mo Kα radiation ($\bar{\lambda}$ = 0.71069 Å, graphite monochromator), $\omega/2\theta$ scan up to an angle of $\theta = 30°$ ($0 \le h \le 15$, $0 \le k \le 31$, $-16 \le l \le 16$), maximum scan time 90 s/reflection. The lattice constants were calculated from the Bragg angles of 25 centered reflections (Mo Kα_1, λ = 0.70926 Å). In addition, the temperature dependence of the lattice constants was measured in the range 110 K up to room temperature. The intensities were Lp-corrected and normalized by a linear regression of the measured intensities of three standard reflections (variation 0.02 at 215 K/0.12 at 124 K). After the data were set on an absolute scale with a K-curve[13] and equivalent reflections were eliminated (R_{int} = 0.016/0.35) there remained 7481/3598 reflections. Among them 3239/2105 with $I < 2\sigma(I)$ were classified as weak and set to $I = 0.5\sigma(I)$. An absorption correction could not be applied, because the crystal was destroyed after data collection. Therefore, the exact size could not be determined. However, as the crystal was nearly a cube and μ = 36.16 cm^{-1} is not too high, absorption correction can be neglected without lack of accuracy. The crystal data for the HS state at 215 K are listed in Table I, the temperature variation data of the lattice constants in Table II. The errors in Table II are only the statistical errors of calculating the lattice constants from the 25 reflections at each temperature, whereas the errors given in Table I are adopted from a linear regression of the temperature variation of lattice constants in the high-temperature range.

Solution and Refinement of the HS Structure. All atoms of $[Fe(2\text{-pic})_3]Br_2 \cdot EtOH$ occupy the general equivalent position 4e of the space group $P2_1/n$. The positional parameters of the three heavy atoms Fe, Br1, and Br2 were determined from a three-dimensional Patterson synthesis. The positions of all other non-hydrogen atoms could be determined by Fourier synthesis and all hydrogen positions of the ligands by difference Fourier syntheses. Only the hydrogen positions of the ethanol molecule had to be calculated and they were treated as rigid groups (CH_3, CH_2, fixed O–H bond distance). Their positional parameters are included in the supplementary material.[19]

The structure was refined with the method of least squares (minimum of $\sum w(|F_o| - |F_c|)^2$). Scattering factors were used for C, N, and O from Cromer and Mann[14] and for Br and Fe from Doyle and Turner;[15] anomalous scattering factors were taken from Cromer and Liberman.[16] All non-hydrogen atoms were calculated anisotropically; the hydrogen atoms were calculated isotropically with a common temperature coefficient of 0.048 for all hydrogen atoms of the ligands. The structure could be refined to a reliability index $R = (\sum||F_o| - |F_c||)/\sum|F_o| = 0.050$ and a weighted index of $R_w = ((\sum w(|F_o| - |F_c|)^2)/\sum w|F_o|^2)^{1/2} = 0.079$ with $w^{-1} = (\sigma^2(F_o) + 0.0098F_o^2)$. Table III contains the positional parameters with estimated standard deviations. The coefficients of the temperature factors are included in the supplementary material.[19]

The second intensity data set collected at 124 K ($0 \le h \le 15$, $0 \le k \le 13$, $-16 \le l \le 16$) could not be completed because of fading intensities. Probably the crystal was deadjusted due to icing. The statistical errors of the data are larger than those found at room temperature. This is due to the fact that in the low-temperature range the crystal contains large HS and small LS molecules with corresponding changes of the identity periods. This is verified by the diffuse shape of the reflections on the Weissenberg photographs. The effect is much stronger in the bromide compound than in the chloride compound because of the rather big volume change upon spin transition (twice as much as in the chloride). Under these circumstances an exact structure determination is not possible. Nevertheless, we have verified the same structure as at room temperature within the limits of error ($R = 0.27$, $R_w = 0.30$ for isotropic refinement). As the systematic absences remain unchanged, we assume the space group $P2_1/n$ to be the right one. In spite of this there could be a slight possibility that it is only a pseudosymmetry. So we calculated structure refinements based on the space groups Pn and $P2_1$, which resulted, however, in unrealistic bond lengths and temperature factors.

All calculations were carried out with an HB 66/80 computer using the program SHELX-76[17] for the structural calculations and the program PLUTO-78[18] for the molecular and structural drawings. A list of measured and calculated structure factors (215 K) is available.[19]

3. Mössbauer Measurements. The Mössbauer spectra were recorded in transmission geometry by using a $^{57}Co/Rh$ source kept at room temperature and a conventional spectrometer operating in the constant-acceleration mode. The samples (~0.15 mg $^{57}Fe/cm^2$) were sealed in poly(methyl methacrylate) containers and placed in a bath cryostat. The temperature stability was ca. 0.1 K.

Figure 1 shows two spectra measured at 125.5 K and near room temperature (280 K). The spectrum at 125.5 K shows two quadrupole doublets; the two outer lines belong to the quadrupole doublet of the HS state and the inner two lines to that of the LS state. The line width of both doublets is only slightly broadened by thickness effects, so that relaxation effects between HS and LS can be excluded and the areas of the HS and LS doublets can be considered proportional to the fraction of the complex molecules in their respective spin states. The spectrum near room temperature shows only the typical HS quadrupole doublet, so that $\gamma(T_R) = 1$.

(9) Greenaway, A. M.; O'Connor, C. J.; Schrock, A.; Sinn, E. *Inorg. Chem.* **1979**, *18*, 2692.
(10) Mikami, M.; Konno, M.; Saito, Y. *Acta Crystallogr., Sect. B: Struct. Crystallogr. Cryst. Chem.* **1980**, *B36*, 275.
(11) Meissner, E.; Köppen, H.; Spiering, H.; Gütlich, P. *Chem. Phys. Lett.* **1983**, *95*, 163.
(12) Köppen, H.; Müller, E. W.; Köhler, C. P.; Spiering, H.; Meissner, E.; Gütlich, P. *Chem. Phys. Lett.* **1982**, *91*, 348.
(13) Karle, J.; Hauptman, H.; Christ, C. L. *Acta Crystallogr.* **1958**, *11*, 757.
(14) Cromer, D. T.; Mann, J. B. *Acta Crystallogr. Sect. A: Cryst. Phys., Diffr., Theor. Gen. Crystallogr.* **1968**, *A24*, 321.
(15) Doyle, P. A.; Turner, P. S. *Acta Crystallogr., Sect. A: Cryst. Phys., Diffr., Theor. Gen. Crystallogr.* **1968**, *A24*, 390.
(16) Cromer, D. T.; Liberman, D. *J. Chem. Phys.* **1970**, *53*, 1891.
(17) Sheldrick, G. *SHELLX-76, Program for Crystal Structure Determination*, University of Cambridge, 1976.
(18) *Cambridge Crystallographic Database, PLUTO-78*, University of Cambridge; Version of Aug 1981.
(19) Supplementary material.

Table II. Temperature Dependence of the Lattice Constants of [Fe(2-pic)$_3$]Br$_2$·EtOH

T, K	a, Å	b, Å	c, Å	β, deg	V, Å^3
294	11.151 (3)	22.356 (4)	11.839 (3)	117.77 (2)	2611 (1)
221	11.161 (3)	22.261 (5)	11.700 (2)	117.95 (2)	2568 (1)
217	11.168 (4)	22.256 (6)	11.725 (2)	118.05 (3)	2572 (1)
215	11.164 (4)	22.281 (4)	11.713 (2)	118.02 (2)	2572 (1)
208	11.161 (3)	22.252 (5)	11.695 (2)	118.00 (2)	2564 (1)
200	11.188 (9)	22.254 (16)	11.676 (8)	117.98 (6)	2567 (4)
192	11.163 (3)	22.239 (8)	11.676 (4)	117.99 (3)	2560 (2)
177	11.166 (3)	22.211 (5)	11.647 (4)	118.01 (3)	2550 (1)
161	11.164 (3)	22.203 (7)	11.623 (3)	118.01 (2)	2543 (1)
144	11.155 (3)	22.171 (6)	11.601 (3)	118.05 (3)	2532 (1)
131	11.151 (3)	22.135 (8)	11.589 (4)	118.00 (3)	2526 (1)
124	10.907 (22)	22.026 (26)	11.554 (22)	117.56 (20)	2461 (9)
124	10.886 (36)	22.007 (32)	11.549 (39)	117.41 (28)	2456 (14)
116	10.854 (39)	22.018 (42)	11.467 (29)	117.12 (27)	2439 (13)
106	10.832 (59)	22.008 (42)	11.457 (47)	117.57 (42)	2421 (20)

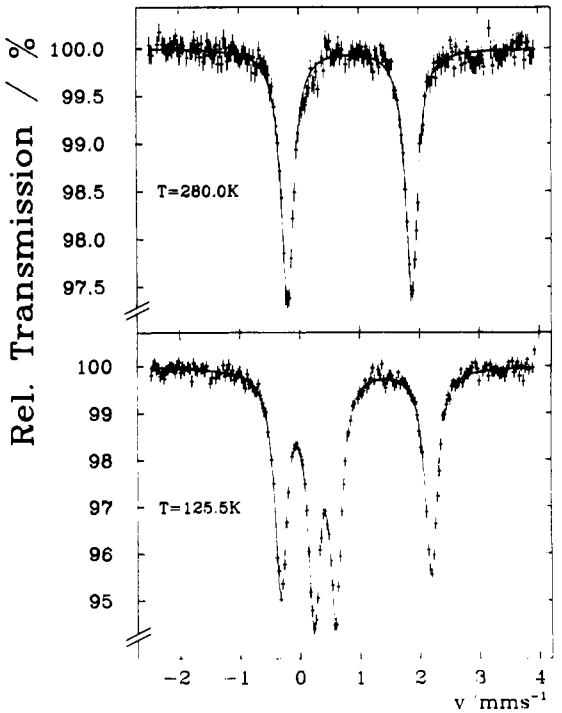

Figure 1. Mössbauer spectra of [Fe(2-pic)$_3$]Br$_2$·EtOH at 280 K and at 125.5 K.

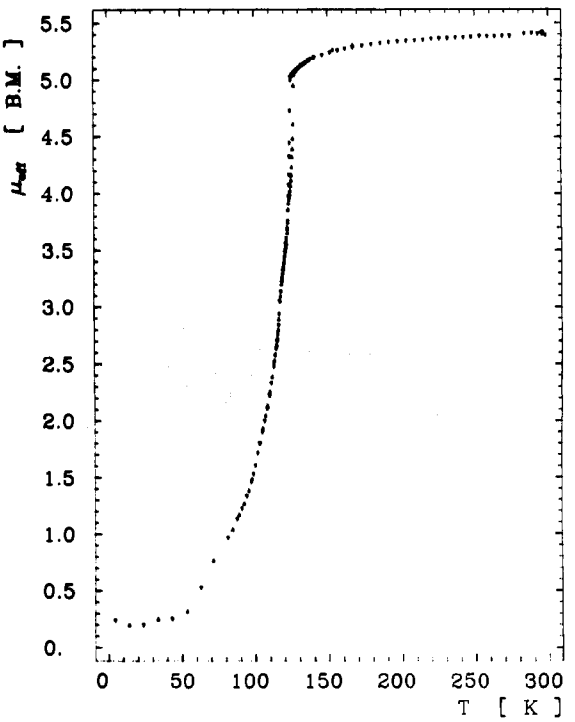

Figure 2. Temperature dependence of the effective magnetic moment μ_{eff} of [Fe(2-pic)$_3$]Br$_2$·EtOH.

4. Susceptibility Measurements. The magnetic susceptibility χ of [Fe(2-pic)$_3$]Br$_2$·EtOH was measured at 10 kOe by using a FONER-type magnetometer equipped with a helium-flow cryostat. The temperature of the sample was measured by using a thermocouple of 0.03% iron in gold vs. 10% chromium in nickel. The temperature stability was better than 0.05 K. The diamagnetic correction was determined by using the magnetic susceptibility of [Zn(2-pic)$_3$]Cl$_2$·EtOH (-460×10^{-6} emu). In Figure 2 the $\mu_{eff} = 2.828(\chi_{cor}T)^{1/2}$ values are plotted in the temperature range between 40 K and T_R = 298 K.

Results and Discussion

1. Crystal and Molecular Structure. The crystal structure of [Fe(2-pic)$_3$]Br$_2$·EtOH is isomorphous to that of the analogous chloride compound, which has already been described in the literature.[9,10] Some essential features of the bromide and the chloride are pointed out here. The complex [Fe(2-pic)$_3$]$^{2+}$ exists solely in meridional configuration. This means that the pyridine and amino nitrogen atoms of the three nonequivalent ligands occupy the corners of the distorted octahedral FeN$_6$ polyhedron such that there is only a 2-fold symmetry (Figure 3). Furthermore, all three picolylamine ligands act differently in building up the structure. Figure 4 shows a complete molecule (the asymmetric unit) and the nomenclature used. Table IV contains the bond distances and the essential bond angles. The C–C and C–N bond distances of the three ligands are not significantly different, either from one another or from those of the corresponding chloride structure.[9] In the chloride HS structure the

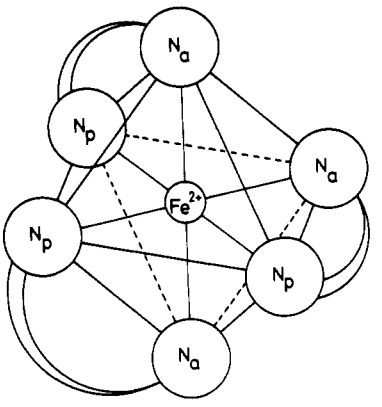

Figure 3. Coordination polyhedron of the FeN$_6$ core, indicating the chelate rings from pyridine nitrogen to amino nitrogen.

pyridine nitrogen distances to iron are significantly larger (0.03 Å) than the amino nitrogen distances. In the bromide structure this tendency is observed only in ligand 1, where the Fe–N distances are 2.223 (pyridine) and 2.181 Å (amino), respectively.

The [Fe(2-pic)$_3$]$^{2+}$ ion is linked centrosymmetrically to its enantiomer by the hydrogen bond N1–H8···Br1 (3.423 Å) of ligand 1. The amino group of ligand 2 bridges with either hy-

Table III. Positional Parameters x, y, and z (with Esd's in Parentheses) of $[Fe(2\text{-pic})_3]Br_2 \cdot EtOH$

atom	x	y	z	atom	x	y	z
Br1	0.29343 (5)	0.06692 (2)	0.44222 (5)	Fe1	0.71690 (7)	0.13465 (3)	0.69949 (7)
Br2	0.68010 (6)	0.27738 (3)	0.42840 (6)				
			Ligand 1				
N11	0.6169 (5)	0.0496 (2)	0.6924 (4)	C31	0.9648 (8)	0.0399 (3)	1.1358 (6)
N21	0.8323 (5)	0.0973 (2)	0.8979 (4)	C41	0.8379 (3)	0.0216 (3)	1.0413 (7)
C11	0.9541 (6)	0.1156 (3)	0.9877 (6)	C51	0.7750 (6)	0.0495 (3)	0.9248 (5)
C21	1.0229 (7)	0.0886 (3)	1.1077 (6)	C61	0.6371 (7)	0.0306 (3)	0.8204 (6)
			Ligand 2				
N12	0.5877 (5)	0.1405 (2)	0.4908 (4)	C32	0.9959 (8)	0.0747 (3)	0.4912 (9)
N22	0.8489 (5)	0.1053 (2)	0.6195 (5)	C42	0.8569 (8)	0.0780 (3)	0.4256 (7)
C12	0.9852 (6)	0.1021 (3)	0.6829 (7)	C52	0.7857 (6)	0.0936 (2)	0.4915 (5)
C22	1.0618 (7)	0.0875 (3)	0.6208 (9)	C62	0.6334 (7)	0.0964 (3)	0.4248 (6)
			Ligand 3				
N13	0.8220 (5)	0.2215 (2)	0.7472 (5)	C33	0.4360 (8)	0.2745 (3)	0.8044 (8)
N23	0.5835 (5)	0.1940 (2)	0.7392 (4)	C43	0.5677 (7)	0.2870 (3)	0.8343 (7)
C13	0.4546 (6)	0.1834 (3)	0.7096 (6)	C53	0.6391 (5)	0.2457 (2)	0.8000 (5)
C23	0.3764 (7)	0.2215 (3)	0.7391 (7)	C63	0.7851 (6)	0.2573 (3)	0.8312 (7)
			Ethanol				
O1	0.8917 (14)	0.3893 (5)	0.5767 (14)	C8	1.0772 (12)	0.3419 (6)	0.5712 (11)
C7	0.9736 (18)	0.3931 (6)	0.5245 (17)				
			Ligand 1				
H11	0.9780 (74)	0.1507 (34)	0.9629 (65)	H51	0.5602 (74)	0.0545 (32)	0.8378 (67)
H21	1.1202 (75)	0.1076 (33)	1.1720 (63)	H61	0.6414 (72)	−0.0116 (33)	0.8167 (65)
H31	0.9936 (73)	0.0197 (33)	1.2028 (68)	H71	0.5259 (80)	0.0482 (33)	0.6308 (69)
H41	0.8144 (81)	−0.0039 (36)	1.0535 (74)	H81	0.6422 (73)	0.0212 (34)	0.6516 (65)
			Ligand 2				
H12	1.0308 (74)	0.1082 (33)	0.7814 (68)	H52	0.6032 (74)	0.1045 (31)	0.3312 (68)
H22	1.1556 (80)	0.0927 (32)	0.6749 (64)	H62	0.5964 (75)	0.0581 (33)	0.4310 (67)
H32	1.0462 (74)	0.0665 (30)	0.4451 (67)	H72	0.6048 (73)	0.1872 (32)	0.4392 (65)
H42	0.8097 (76)	0.0706 (32)	0.3444 (73)	H82	0.4969 (77)	0.1228 (31)	0.4589 (64)
			Ligand 3				
H13	0.4028 (75)	0.1556 (33)	0.6413 (65)	H53	0.7951 (74)	0.2939 (36)	0.8382 (67)
H23	0.2944 (80)	0.2165 (32)	0.7195 (69)	H63	0.8691 (74)	0.2482 (32)	0.9310 (69)
H33	0.3831 (76)	0.2955 (33)	0.8284 (67)	H73	0.7905 (76)	0.2400 (32)	0.6723 (71)
H43	0.6209 (75)	0.3257 (32)	0.8828 (64)	H83	0.8967 (84)	0.2235 (33)	0.7811 (76)

Table IV. Bond Distances (Å) and Bond Angles (deg) of $[Fe(2\text{-pic})_3]Br_2 \cdot EtOH$

	ligand 1	ligand 2	ligand 3		ligand 1	ligand 2	ligand 3
N2–C1	1.333 (7)	1.345 (8)	1.333 (9)	N2–C1–C2	122.8 (7)	122.4 (7)	124.2 (5)
C1–C2	1.383 (9)	1.397 (14)	1.373 (11)	C1–C2–C3	119.0 (6)	118.9 (7)	117.7 (7)
C2–C3	1.382 (12)	1.370 (13)	1.394 (9)	C2–C3–C4	117.3 (6)	119.1 (10)	119.4 (8)
C3–C4	1.388 (9)	1.373 (11)	1.370 (12)	C3–C4–C5	121.3 (7)	119.7 (7)	118.9 (6)
C4–C5	1.358 (9)	1.386 (13)	1.394 (10)	C4–C5–N2	121.1 (5)	122.0 (6)	122.2 (6)
C5–N2	1.354 (8)	1.349 (8)	1.344 (7)	C5–N2–C1	118.4 (5)	117.9 (7)	117.5 (6)
C5–C6	1.508 (8)	1.503 (9)	1.516 (9)	N2–C5–C6	116.5 (5)	116.3 (6)	116.8 (6)
C6–N1	1.470 (9)	1.482 (9)	1.468 (10)	C5–C6–N1	110.8 (6)	109.9 (4)	110.8 (5)
Fe–N1	2.181 (5)	2.182 (5)	2.194 (5)	N1–Fe–N2	75.5 (2)	76.2 (2)	75.6 (2)
Fe–N2	2.223 (5)	2.185 (7)	2.198 (6)				
O1–C7	1.320 (31)			N11–Fe–N22	99.2 (2)		
C7–C8	1.532 (20)			N11–Fe–N23	98.3 (2)		
				N12–Fe–N21	161.4 (2)		
				N12–Fe–N23	92.5 (2)		
				N13–Fe–N21	94.9 (2)		
				N13–Fe–N22	89.2 (2)		

drogen atom to the ions Br1 and Br2. The ethanol molecule is also clearly oriented toward the Br2 ion (distance O–H···Br2 = 3.311 Å). Whereas these three hydrogen contacts are along the monoclinic axis, the amino groups of ligands 3 are linked via Br2 ions in the direction [101], which is the direction of the translation of the glide plane n. Table V contains the data of the hydrogen bonds, and Figure 5 illustrates their locations. All hydrogen bonds correspond to those of the analogous chloride structure. The differences in numerical values are accounted for by the different ionic radii of Br^- and Cl^-. The described 2-dimensional hydrogen bond network builds up layers parallel to the $(\bar{1}01)$ plane, which correspond not only to morphology (large $\{\bar{1}01\}$ faces) but also to the cleavage (only parallel $(\bar{1}01)$).

A peculiarity was observed in the chloride compound concerning the position of the ethanol molecules. Mikami et al.[4,9] found a rotational disorder of the ethanol molecule, which occupies three different sites with one common carbon atom. The population ratio of the disordered ethanol is 3:2:2 at 298 K. In the structure

Table V. Hydrogen Bonds (Å) of $[Fe(2\text{-pic})_3]Br_2 \cdot EtOH$[a]

	Br–H	H–N	Br···N
Br1···H71–N11 (1)	2.53 (6)	0.93 (7)	3.440 (5)
Br1···H81–N11 (3′)	2.51 (8)	0.91 (9)	3.423 (6)
Br1···H82–N12 (1)	2.52 (9)	0.98 (8)	3.472 (6)
Br2···H72–N12 (1)	2.21 (8)	1.26 (8)	3.406 (6)
Br2···H73–N13 (1)	2.66 (8)	0.88 (8)	3.528 (7)
Br2···H83–N13 (2″)	2.80 (8)	0.74 (8)	3.538 (6)
Br2···H91–O	2.20 (13)	1.13 (13)	3.311 (12)

[a] Definition of symmetry positions (compare with Table I): 1 = (1; 0, 0, 0), 2″ = (2; −1, 0, −1), 3′ = (3; 1, 0, 1).

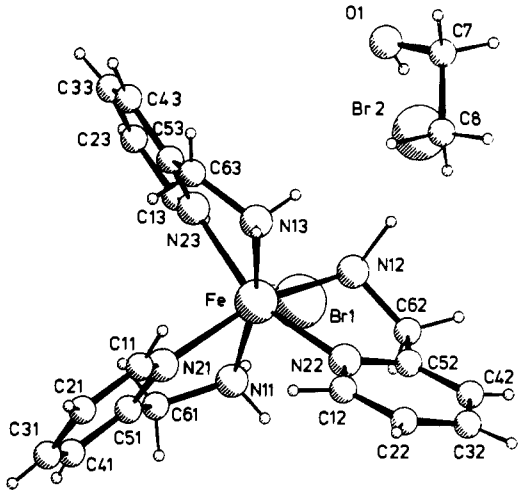

Figure 4. Configuration of the molecule [Fe(2-pic)$_3$]Br$_2$·EtOH and numbering scheme of atoms.

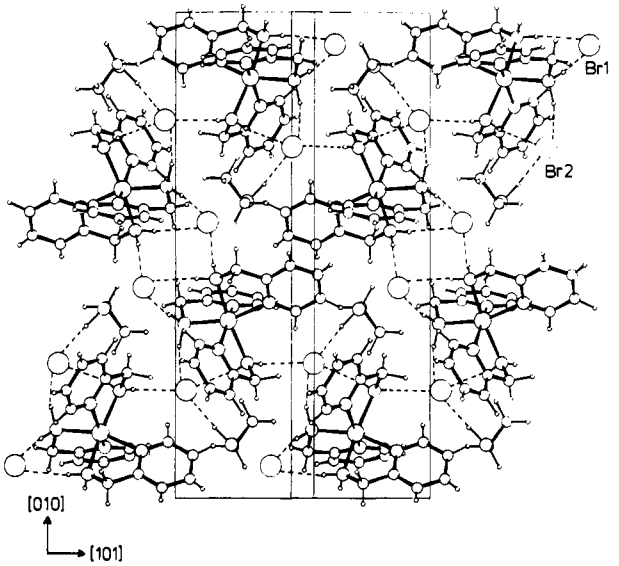

Figure 5. Projection of the unit cell of [Fe(2-pic)$_3$]Br$_2$·EtOH along ($\bar{1}$01), showing the hydrogen bonds (dashed lines).

of the LS Fe^{2+} complex below the transition temperature of 120 K, no disorder was observed. This disorder contributes to the entropy by $\Delta S \approx 8.9$ J mol^{-1} K^{-1},[4] which is roughly the same contribution as the pure spin entropy change of 14.3 J mol^{-1} K^{-1}, and led the authors to the conclusion that this order–disorder transition triggers the gradual high-spin ↔ low-spin transition.

For the bromide compound, which even shows a hysteresis in the temperature dependence of the HS fraction γ, no disorder phenomena can be observed and a Weissenberg photograph with a long exposure time (10 days, Fe Kα radiation) at room temperature shows only sharp reflections. This is even true for those reflections that are mainly produced by the ethanol molecule (e.g. ($\bar{2}$11), and ($\bar{2}$31), (270)). So, a positional disorder seems not to be a reasonable explanation of the too short C–O distance in the solvent molecule. On the other hand the ethanol molecules occupy positions between the [Fe(2-pic)$_3$]Br$_2$ layers, each in the middle of a cage formed by four pyridine rings, three of them being nonequivalent (average distance C7–plane[20] of pyridine ring = 3.86 Å). This seems to explain the rather high temperature factors of the ethanol molecule. Changes in the structure apart from the thermal expansion and the expansion due to the change in bond

(20) The equations of the least-squares planes of the pyridine rings relevant for the ethanol surroundings and the distances of the ethanol atoms from these planes are deposited.[19]

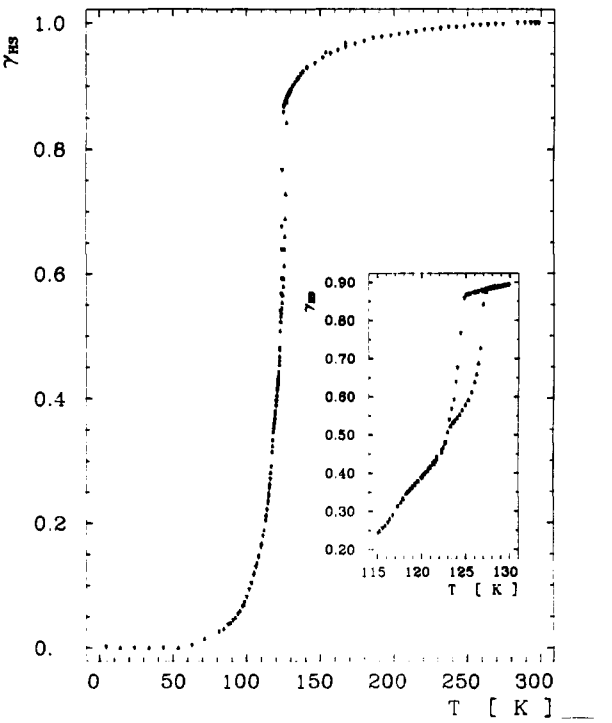

Figure 6. Temperature dependence of the high-spin fraction $\gamma(T)$ of [Fe(2-pic)$_3$]Br$_2$·EtOH. The inset shows the hysteresis region on an enlarged scale.

Table VI. Tensor Elements of Thermal Expansion and Deformation due to the HS–LS Transition, Referred to Their Principal Axes, of [Fe(2-pic)$_3$]Br$_2$·EtOH and [Fe(2-pic)$_3$]Cl$_2$·EtOH and the Angle δ (Clockwise) between the Crystallographic $\vec{a}$ Axis and the $\vec{x}$ Axis of the Principal Axis System[a]

	Br^-	Cl^-
ϵ_1	4.45	2.93
ϵ_2	1.03	1.57
ϵ_3	−0.19	−2.07
Tr(ϵ)	5.29	2.43
$\delta(\epsilon)$	−1	14
η	0.45	1.72
α_1	1.54	1.86
α_2	0.53	0.31
α_3	−0.30	−0.31
Tr(α)	1.77	1.86
$\delta(\alpha)$	97	107

[a] The anisotropy parameter η of the tensor ϵ is defined by $\eta = (\epsilon_2 - \epsilon_3)/(\epsilon_1 - \mathrm{Tr}(\epsilon)/3)$. Units: δ, deg; ϵ_i, 10^{-2}; α_i, 10^{-4} K^{-1}.

lengths are negligible in the bromide, contrary to the isomorphous chloride. Thus far, there is no evidence for a correlation of the hysteresis of $\gamma(T)$ in this compound and special structural changes.

2. Tensor of Thermal Expansion. The basic assumption of the theoretical model,[3] which has occasionally been named the lattice expansion model, is the proportionality of the volume change in the HS–LS transition to the fraction $\gamma(T)$ of HS complex molecules. The unit cell volume of the compound [Fe(2-pic)$_3$]Cl$_2$·EtOH could be described[11] by

$$V(T) = V_{LS}\alpha_v T + \gamma V_{HS} + (1 - \gamma)V_{LS} \quad (3)$$

The thermal expansion is a superposition of the change in $\gamma(T)$ and a linear volume change with temperature. The generalization of this formula, which accounts for the anisotropy of the expansion of the lattice, uses tensors: the tensor of thermal expansion α instead of the scalar α_v and the tensor of deformation ϵ by a HS–LS transformation instead of $(V_{HS} - V_{LS})/V_{LS}$. The temperature dependence of a vector $\vec{x}(T)$ is then given by

$$\vec{x}(T) = (1 + \alpha T + \epsilon\gamma(T))\,\vec{x}(T = 0) \quad (4)$$

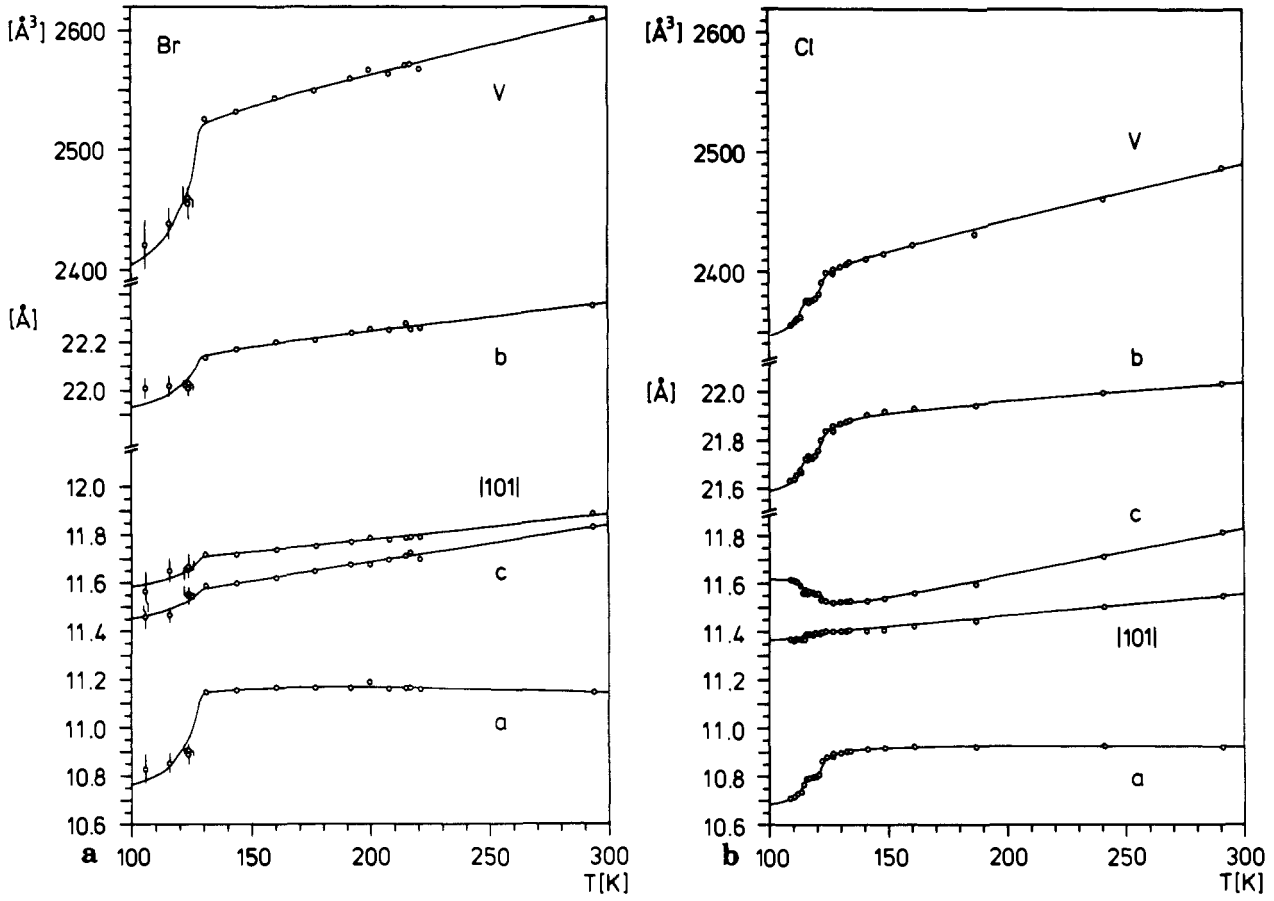

Figure 7. Temperature dependence of the lattice constants and the unit cell volume of (a) $[Fe(2\text{-pic})_3]Br_2 \cdot EtOH$ and (b) $[Fe(2\text{-pic})_3]Cl_2 \cdot EtOH$. Solid lines are calculated curves (error bars for measured values are only given if they exceed the size of the drawn data points).

The traces of the tensors α and ϵ are the scalars α_v and $(V_{HS} - V_{LS})/V_{LS}$, respectively. The HS fraction $\gamma(T)$ has been determined by the temperature dependence of the susceptibility, which is the weighted sum of χ_{HS} and χ_{LS} of the d electrons of the Fe^{2+} ion in the HS and the LS state, respectively:

$$\chi(T) = \gamma(T)\,\chi_{HS}(T) + (1 - \gamma(T))\chi_{LS} \qquad (5)$$

For the susceptibility of the d electrons in the HS state a Curie law behavior $\chi_{HS}(T)\ T = \text{const}$ is assumed. χ_{LS} is taken to be independent of temperature. The Mössbauer measurement at room temperature (T_R) shows no LS fraction, so that $\gamma(T_R) = 1$ and the Curie constant is $\chi(T_R)\ T_R$. In Figure 6 the HS fraction $\gamma(T)$ of $[Fe(2\text{-pic})_3]Br_2 \cdot EtOH$ is plotted vs. temperature. The corresponding curve for the analogous chloride compound has already been published.[12] These $\gamma(T)$ values were used to fit the length of the unit cell vectors. The solid lines in Figure 7 were calculated according to

$$|\vec{x}(T)| = |\vec{x}_0|(1 + (\vec{x}_0{}^T\alpha\vec{x}_0/|\vec{x}_0|^2)T + (\vec{x}_0{}^T\epsilon\vec{x}_0/|\vec{x}_0|^2)\gamma(T)) \qquad (6)$$

In the case of the bromide compound the $\gamma(T)$ values of the cooling curve in Figure 6 have been used. The tensor components are easily evaluated, since one principal axis is already defined by the 2-fold $\vec{b}$ axis of the crystal. This axis is chosen to be the $\vec{y}$ axis of the principal axis system. The temperature dependence of the length of the three axes ($|\vec{a}|$, $|\vec{c}|$ and $|\vec{a} + \vec{c}|$ were used) determines the principal axes in the plane normal to the $\vec{b}$ axis. In Table VI the principal values of the ϵ and α tensors and the angle δ between the $\vec{a}$ axis of the crystal system and the $\vec{x}$ axis of the principal axis system are tabulated for both compounds.

The excellent agreement between the calculated and measured unit cell lengths in Figure 7 proves the basic assumption of the so-called lattice expansion model[3] in a most general form to be correct. The deformation and expansion of the lattice is strongly proportional to the number of complexes in the HS and LS state. This is true for both compounds. The order–disorder transition in the chloride compound obviously has no observable effect on the deformation of the lattice, so that the assumption of a strong coupling between the LS–HS and the order–disorder transition is not justified. The hysteresis of $\gamma(T)$ of the bromide compound is therefore supposed to be only a result of the stronger interaction Γ between the HS complex molecules. Γ is proportional to the square of ΔV_{HL}, the difference of HS and LS volume (eq 2). This difference is proportional to $\mathrm{Tr}(\epsilon)$, which is indeed much larger for the bromide than for the chloride compound (cf. Table VI).

This detailed consideration of the lattice expansion raises new questions. The α tensors of both compounds are very similar as is expected for isomorphous structures. The ϵ tensors, however, are different. Their traces differ by a factor of 2. This fact conflicts with the idea that only the change of the volume and the shape of the complexes $[Fe(2\text{-pic})_3]^{2+}$ on going from the LS to the HS state is responsible for the expansion of the crystal. Since this complex is the same in both compounds, which are isomorphous, similar ϵ tensors should also be expected. The question whether this expectation is wrong or whether the change of the volume and the shape of the complexes is so much influenced by the neighborhood of a chloride or a bromide anion needs further investigation. In the framework of the lattice expansion model[3] there arises another difficulty. The difference of the volume change by a factor of 2 is too large to explain the small hysteresis of 2 K and the small shift of the transition temperature. Simulation of transition curves according to eq 1 shows that an increase of Γ by less than 10% as compared to the value used for the chloride compound reproduces a small hysteresis of the $\Gamma(T)$ curve. An increase of the volume change by a factor of 2, however, leads to an increase of Γ by a factor of 4 in the frame of the lattice expansion model (eq 2). There may be a way out of this difficulty. If Γ also essentially depends on the anisotropy η of the ϵ tensor and not only on the trace, the larger anisotropy of ϵ of the chloride compound may compensate the larger trace of ϵ of the bromide compound. An extension to the lattice expansion model seems

therefore to be necessary.

Acknowledgment. We thank the Deutsche Forschungsgemeinschaft, the Stiftung Volkswagenwerk, and the Fonds der Chemischen Industrie for financial support.

Registry No. $[Fe(2\text{-pic})_3]Br_2 \cdot EtOH$, 71521-13-6.

Supplementary Material Available: Listings of structure factor amplitudes, anisotropic temperature factors, calculated hydrogen positions of the ethanol molecule, and least-squares planes of the pyridine rings (27 pages). Ordering information is given on any current masthead page.

Contribution from the Institute of Inorganic Chemistry, University of Münster, D-4400 Münster, Federal Republic of Germany, and Chemistry Department A, Technical University of Denmark, DK-2800 Lyngby, Denmark

Crystal Structure and Infrared and Raman Spectra of $KV(SO_4)_2$

Rasmus Fehrmann,*[1a] Bernt Krebs,[1b] G. N. Papatheodorou,[1c,d] Rolf W. Berg,[1a] and Niels J. Bjerrum[1a]

Received July 31, 1985

Green $KV(SO_4)_2$ crystals were synthesized by dissolution of V_2O_5 in a $KHSO_4$ melt at 450 °C under SO_2(g) atmosphere. Slow cooling of the solution from 450 to 250 °C in 3 weeks gave small crystals that were used for X-ray structure determination and for obtaining oriented-crystal Raman and infrared spectra. The crystal structure, in rhombohedral (trigonal) space group $R\bar{3}$ with $a = b = 4.781$ (1) Å and $c = 23.545$ (5) Å at −130 °C and $Z = 3$, consists of a unique arrangement of tetrahedral SO_4^{2-} linked to octahedrally coordinated vanadium(III). The structure is compared to other closely related $M^IM^{III}(SO_4)_2$ structures. Infrared spectra on powder and on crystals along c could be assigned conclusively. Raman spectra were measured from small oriented single crystals by using different light polarizations. Anomalous polarization and preresonance enhancement of certain Raman bands were observed. Ten Raman-active modes were predicted by group-theoretical analysis whereas the experiments showed the presence of eleven bands. The extra band at ~1560 cm^{-1} was attributed to a d ← d electronic Raman transition, ν_e, $^3E_g \leftarrow {}^3A_g$, of vanadium(III) in the trigonal crystal field.

Introduction

The chemistry of vanadium(V) oxide dissolved in molten $KHSO_4$–$K_2S_2O_7$ mixtures has been thoroughly investigated[2-6] due to the catalytic importance of these melts in the commercial oxidation of SO_2 to SO_3 for the production of sulfuric acid.[7] During the work[6] we unexpectedly discovered the formation of a green precipitate, which proved to be crystals of $KV(SO_4)_2$. Apparently this compound, mentioned previously in the literature,[8-11] seems to have a quite low solubility not only as known in aqueous sulfuric acid solutions but also in $KHSO_4$–$K_2S_2O_7$ melts in equilibrium with a SO_2 atmosphere. The pressure- and temperature-dependent solubility of $KV(SO_4)_2$ is presently under investigation and will be reported elsewhere.[6]

The present work is concerned with the fundamental properties of the $KV(SO_4)_2$ compound. The crystal structure is determined, the selection rules and correlation diagram for the vibrational properties of the crystal are derived, and the Raman and infrared spectra are presented and assigned according to the group-theoretical considerations.

Synthesis of Crystalline $KV(SO_4)_2$

The green compound, $KV(SO_4)_2$ has previously been prepared (i) by concentrating sulfuric acid solutions containing potassium and vanadium,[8,9] (ii) by bubbling SO_2 gas through potassium pyrosulfate–potassium vanadate melts,[10] and (iii) by tempering a finely ground 1:1 solid mixture of K_2SO_4 and $V_2(SO_4)_3$.[11]

The possibility of isolating the salt from $KHSO_4$ melts containing dissolved vanadium oxides under a SO_2 atmosphere was discovered during our spectroscopic investigations,[6] where bright green crystals appeared in the spectroscopic cuvettes.

In order to prepare large single crystals suitable for X-ray structure and spectroscopic investigations, long-term precipitation procedures were followed: $KHSO_4$ and V_2O_5 or V_2O_4 were added to Pyrex ampules (molar fraction X_{KHSO_4} = ca. 0.983) that were sealed off under 0.9 atm of SO_2.

As described previously,[4] the $KHSO_4$ used was from Merck (Suprapure or Pro Analysi) and was dried at 110 °C for 3 days and subsequently stored and handled in a glovebox with dry-nitrogen atmosphere. V_2O_5 and V_2O_4 from Cerac (Pure, 99.9 and 99.5%, in the form of sized nonhygroscopic granules) were used without further purification. The purity of SO_2 was better than 98% by volume. After fusion and equilibration at 450 °C, the melts had formal concentrations of vanadium at ~0.5 mol/L, based on the known density.[3]

The ampules had estimated gas to melt volume ratios sufficiently large to secure an excess of SO_2 even after complete reduction to V(III) of the vanadium present. Bright green solutions were obtained within a few hours. The speed of dissolution seemed much faster for V_2O_5 than for V_2O_4. The latter oxide probably dissolves through a redox process since a gas (possibly SO_2) was evolved from the contact zone between the melt and solid. The melts were gently rocked overnight at 450 °C, in a Kanthal-wire-wound quartz-tube furnace with a water-cooled glass jacket (temperature precision within 5 °C). Then, the temperature was reduced to 425 °C and kept there for 1 week. A yellow-green crystalline precipitate slowly separated out. The temperature was further gradually reduced to 250 °C in steps of 25 °C during a period of 8 weeks. As the temperature decreased, the color of the melts changed gradually from green to blue, ending up as almost clear at 250 °C, indicating that the melts were nearly completely empty of vanadium.

The crystals were finally isolated by cutting the ampules open and gently flushing the solidified content with water, which slowly during several days dissolved the $KHSO_4$ but not the $KV(SO_4)_2$.

The crystals were examined under a polarization microscope, and proper crystals were selected for the investigations.

The chemical analysis[6] of the compound with respect to V and K was in accordance with the formula $KV(SO_4)_2$.

On heating, the bright green color of $KV(SO_4)_2$ faded toward yellow-green, until the compound finally decomposed at ~450 °C.

X-ray Investigations

Powder Diffraction. The X-ray powder diffraction pattern of a sample quoted to be $KV(SO_4)_2$ has been published by Perret,[11] who indexed his pattern in a monoclinic cell with $a = 8.16_4$ Å, $b = 5.14_8$ Å, $c = 7.87_0$ Å, $\beta = 94°\ 20'$, $Z = 2$, $D_{calcd} = 2.836$ g cm^{-3}, and $D_{exptl} = 2.81$ g cm^{-3}, probably closely analogous to the yavapaiite $KFe(SO_4)_2$ structure[12-14] in space group $C2/m$.

(1) (a) Technical University of Denmark. (b) University of Münster. (c) Institute of Chemical Engineering and High Temperature Processes, University of Patras, Gr-26110 Patras, Greece. (d) Visiting Professor at the Technical University of Denmark in 1984.
(2) Hansen, N. H.; Fehrmann, R.; Bjerrum, N. J. *Inorg. Chem.* **1982**, *21*, 744.
(3) Hansen, N. H.; Bjerrum, N. J. *J. Chem. Eng. Data* **1981**, *26*, 13.
(4) Fehrmann, R.; Hansen, N. H.; Bjerrum, N. J. *Inorg. Chem.* **1983**, *22*, 4009.
(5) Fehrmann, R.; Gaune-Escard, M.; Bjerrum, N. J. *Inorg. Chem.*, in press.
(6) Fehrmann, R.; Hansen, N. H.; Bjerrum, N. J.; Philipsen, J.; Pedersen, E., to be submitted for publication.
(7) Sittig, M. "Sulfuric Acid Manufacture and Effluent Control", Chemical Process Review No. 55; Noyes Data Corp.: Park Ridge, NJ, 1971.
(8) Rosenheim, A.; Mong, H. Y. *Z. Anorg. Allg. Chem.* **1925**, *148*, 25.
(9) Sieverts, A.; Müller, E. L. *Z. Anorg. Allg. Chem.* **1928**, *173*, 313.
(10) Frazer, J. H.; Kirkpatrick, W. J. *J. Am. Chem. Soc.* **1940**, *62*, 1659.
(11) Perret, R. *Bull. Soc. Fr. Mineral. Cristallogr.* **1971**, *94*, 84.
(12) Hutton, C. O. *Am. Mineral.* **1959**, *44*, 1105.
(13) Graeber, E. J.; Rosenzweig, A. *Am. Mineral.* **1971**, *56*, 1917.
(14) Anthony, J. W.; McLean, W. J.; Laughon, R. B. *Am. Mineral.* **1972**, *57*, 1546.

0020-1669/86/1325-1571$01.50/0 © 1986 American Chemical Society